ACS OMEGA

Open Access

http://pubs.acs.org/journal/acsodf

Article

Role of Altitude in Influencing the Spray Combustion Characteristics of a Heavy-Duty Diesel Engine in a Constant Volume Combustion Chamber. Part II: Impinging Diesel Jet

Chengguan Wang, Tao Wang,* Diming Lou,* Piqiang Tan, Zhiyuan Hu, Liang Fang, Rong Yang, and Xiaozhi Qi

Cite This: *ACS Omega* 2024, 9, 4513−4527

Read Online

ACCESS | Metrics & More | Article Recommendations

ABSTRACT: Wall impingement, particularly liquid−wall impingement, has been demonstrated to be one of the critical causes of combustion deterioration in plateau diesel engines. Obviously, the complexity of wall impingement is exacerbated by the plateau scenario. However, fundamental studies specifically dedicated to this phenomenon are still inconclusive and insufficiently detailed, obviating the feasibility of the targeted design and optimization of diesel engines operating in regions with different altitudes. Consequently, the second part of this investigation, presented in this work, focused on the detailed physical and chemical processes of impinging spray combustion under different altitude conditions. A wall impingement system was designed to generate an impinging spray flame. The impingement distance was varied from 77 to 37 mm to cover different situations of wall impingement. The liquid spray, ignition, and combustion processes were visualized in detail by using different optical diagnostics. The results showed that the variation of the liquid length with the impingement distance was mainly dependent on the liquid impingement under the same altitude condition. The effect of the impingement distance on the ignition distance was more sensitive to the altitude. The quantitative analysis of the flame natural luminosity confirmed the decisive effect of the impinging flame morphology on the ambient entrainment and fuel−air mixing under different altitude conditions, and it also revealed that there was an optimal impingement distance under identical altitude conditions to achieve minimum soot emissions. And interestingly, the optimal impingement distance increased with altitude. Finally, the spray combustion processes of an impinging diesel jet were determined to occur in four typical regions, upon which a schematic diagram depicting the flame structure of an impinging diesel jet was proposed to phenomenologically describe the role of altitude in impinging spray combustion processes. Based on this, an attempt was made to explore some new perspectives beyond the popular solutions to recover and improve the performance of plateau diesel engines.

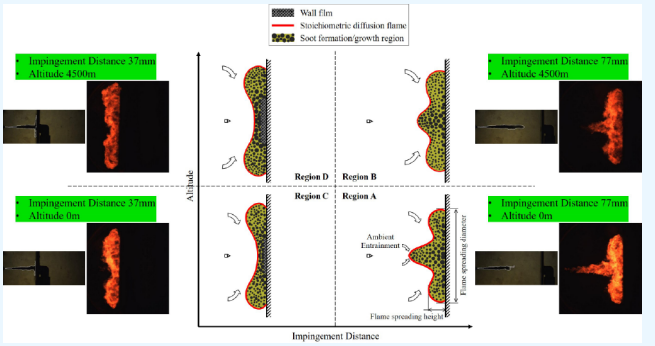

1. INTRODUCTION

Due to their remarkable efficiency, fuel economy, and high reliability, compression ignition (CI) engines have been widely relied upon for transportation, power generation, and other applications over the past century.[1,2] Moreover, with the development and application of low-carbon and carbon-neutral fuels, CI engines are expected to remain indispensable for the foreseeable future.[3] Thus, a deeper understanding of the complex physical and chemical mechanisms for various stages of combustion is still required to design more powerful and efficient engines. It is considered that diesel engines, as a common type of CI engines, provide a primary solution for various economic activities and road transportation especially in plateau regions.[4,5] The inevitable reduction in atmospheric pressure with increasing altitude reduces the density of air inhaled into the cylinder. This affects the propagation and entrainment of the diesel spray, as well as the subsequent mixing-controlled combustion process, all of which have adverse effects on diesel engines.[6] One of the challenges that the engine designers have to address is to ensure engines capable of operating at plateau up to 4500 m without significant performance deterioration.[7] However, the current situation is that most ground vehicle engines are not designed to operate at high altitudes above 3000 m.[8] Indeed, there are

Received: September 23, 2023
Revised: December 12, 2023
Accepted: December 20, 2023
Published: January 19, 2024

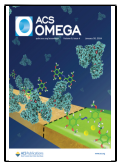

large populations and industrial operations located in high-altitude regions all over the world. Consequently, the topic of plateau performance in diesel engines is noteworthy.

During the past few years, major advances have been made in several encouraging studies to reveal the potential causes of plateau combustion deterioration. It is commonly accepted that the ignition delay is prolonged under higher altitude conditions, leading to a longer premixed combustion duration.[8,9] Accompanied by this phenomenon, some researchers recently noticed that an enhanced pressure rise rate in the premixed combustion stage would result in an abnormal combustion, such as diesel knock, for heavy-duty diesel engines operating in plateau regions, which would cause damage to the combustion chamber and piston crown. Wang et al.[10] conducted optical experiments on diesel knock for high-altitude engines and confirmed that the origin of diesel knock correlated with diesel spray impingement, and they also found that the occurrence of diesel knock was sensitive to a high injection pressure and small combustion chamber, which could be attributed to the spray impingement and premixed mixture formation. In their companion paper,[11] they argued that the knock intensity decreased as the ambient pressure increased under lower altitude conditions for fixed injection pressures satisfying knocking combustion, which was attributed to the weakened liquid spray impingement. Moreover, Li et al.[12] analyzed the effects of the altitude on the combustion characteristics with the large eddy simulation (LES) method and concluded that when the altitude was increased from 0 to 4500 m, the combustion changed from normal combustion to knocking combustion and the combustion efficiency decreased from 90% to 47% due to severe impingement. Another issue caused by the deteriorated combustion encountered in high-altitude operating diesel engines is worsened emissions.[13,14] Continually tightening environmental regulations, which include altitude tests and considering altitude as a new relevant homologation variable, have prompted diesel engine manufacturers to tune engines for high-altitude operating conditions to ensure that emissions do not exceed the limits in both plain and plateau regions.[4,15] Currently, after-treatment systems are widely employed for modern diesel engines to meet current and future emissions regulations. However, the increase in soot emissions of high-altitude diesel engines lead to the failure of after-treatment components.[16] To reduce the risk of failure, Zhang et al.[17] developed a multidimensional computational fluid dynamics (CFD) model to elucidate the mechanism of increased soot emissions from high-altitude operating diesel engines. The changes in the soot concentration in each region where it should form were investigated with variations in the altitude. Interestingly, they provided a soot formation mechanism to prove that an altitude of 3000 m could be regarded as a threshold for a significant increase in soot formation. In this proposed mechanism, a higher likelihood of fuel droplets impinging on the wall would lead to the formation of a liquid film under altitude conditions over 3000 m, and then, the soot emissions sharply increased under altitude conditions above 4000 m. Meng et al.[18] continued to analyze the causes of this phenomenon by means of a CFD model. In other words, they confirmed that liquid impingement is one of the reasons for the sudden degradation of combustion reported by Szedlmayer et al.[8] when a diesel engine was operated above 3000 m.

The aforementioned recent studies have provided insights into the spray combustion process of diesel engines operating in plateau regions, highlighting the importance of wall impingement, particularly liquid−wall impingement. Wall impingement has been a topic of considerable scientific inquiry for years.[19] In the field of diesel engines, the combustion inside the chamber is a complex turbulent process within a confined space, which involves the high-momentum diffusion spray flame impinging on the combustion chamber wall. Previous investigations have achieved great achievements in the visualization of spray flame impingement of diesel engines, and the wall is often simplified to be flat to isolate the impingement phenomenon.[20] In general, the wall impingement can be divided into two categories: spray wall impingement (SWI) and jet wall impingement (JWI).[3] The SWI refers to the situation where the liquid fuel is not completely vaporized before it reaches the wall, while the JWI occurs when the liquid fuel has completely converted to a gaseous state before reaching the wall. Impingement alters the spatio-temporal distributions of the spray and flame, introducing specific phenomena that are not reproducible in a free jet, and therefore significantly influence the mixing, ignition, combustion, and emission processes.[21−23]

Another important concern is that the influence of wall impingement has been shown to be complex. As previously reported by Edwards et al.,[24] the effect of impingement involves at least three components: fluid mechanics, thermal effects, and chemical effects. This kind of complexity introduces various unexpected uncertainties to the impingement, making the fundamental research for the wall impingement to remain as an active topic nowadays.[19,25−27] Nevertheless, complete agreement on the impact of the wall impingement has not yet been reached, some researchers argue that wall impingement facilitates spray combustion and emissions,[23,28−30] while others came to opposite conclusions.[31−34] Some researchers devoted to interpret these contradictory conclusions,[35,36] and one potential explanation depends on whether the wall impingement is SWI or JWI. Wang et al.[37] reported that their configuration corresponded to SWI in the case of conventional nozzles, and hence the liquid wetting effect leads to deteriorated soot formation, while the work of both Xuan et al.,[3] and Pickett and López[21] focused on the JWI cases, showing lower soot level of the impinging spray flame. By varying the impingement distance from 30 to 60 mm, Li et al.[38] identified that the wall impingement deteriorated diesel combustion when SWI occurred, whereas the combustion was observed to be enhanced by increasing the impingement distance, with the wall impingement shifting to JWI cases.

Shifting our focus to the in-cylinder combustion of realistic diesel engines, the influence of the wall impingement becomes more complex in a plateau scenario. On one hand, due to the excessive penetration of the diesel spray and flame resulting from a smaller ambient density, the impingement becomes more prominent with increasing altitude. On the other hand, the engines would experience various altitudes when operating in plateau regions, coupled with the spatial and temporal variations in the distance between the spray tip and the piston cavity wall, making it difficult to directly distinguish between the SWI and JWI. Due to the complex characteristics of wall impingement, the details of impinging spray combustion process of diesel engines operating under different altitude conditions cannot be determined only by speculation and/or extrapolation. Obviously, these details involved make it difficult to make observations in realistic engines. To alleviate this

https://doi.org/10.1021/acsomega.3c07357
ACS Omega 2024, 9, 4513−4527

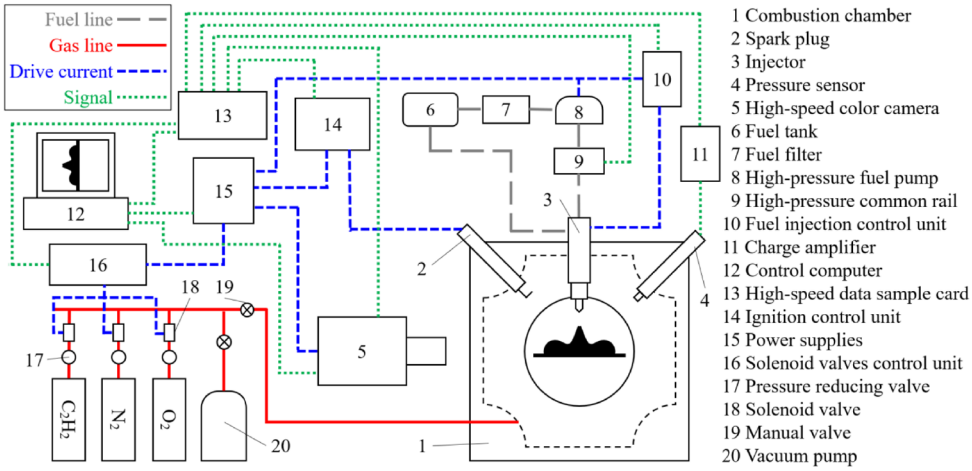

Figure 1. Schematic diagram of the constant volume combustion chamber system.

difficulty, out-of-engine experiments can be adopted to provide the desired fundamental information.[39,40] The CVCC may be the most convenient option since the impingement distances can be easily adjusted to control the wall impingement. However, to the best of the authors' knowledge, few experiments have been performed in CVCC under high-altitude conditions. The lack of available optical visualization results to clarify the differences in the combustion characteristics of diesel engines operating under different altitude conditions motivated Part I of this investigation to accomplish the visualization of free spray combustion under different altitude conditions in a constant volume combustion chamber (CVCC). However, as explained at the end of Part I,[41] the assumption that the spray flame is fully developed is very idealistic, and the conclusions obtained are only applicable to free jets in relatively quiescent ambient conditions. Indeed, one of the core links missing for the transition from this idealistic configuration to a real engine is the interaction between the spray flame and the piston-bowl wall,[35] which is the focus of the present work. In addition, the inevitable impingement provides an additional variable that can be utilized to optimize diesel spray combustion in plateau regions, but the absence of a conclusive understanding of wall impingement impedes its utilization for optimization. To overcome these obstacles, it is of great urgency to conduct in-depth visualization investigations to understand the characteristics of an impinging spray and flame under different altitude conditions comprehensively.

With the above considerations, the present work continues Part I of this investigation with the assumption that the diesel jet develops in a limited domain, aiming to obtain elaborate information on the impinging spray combustion process of heavy-duty diesel engines operating under different altitude conditions by means of standard optical techniques. The CVCC system employed in Part I was modified by adding a wall impingement system in this work. The impingement distance was adjusted from 77 to 37 mm to reproduce the transition from a free jet to an impinging jet (refer to JWI) up to liquid impingement (refer to SWI). Furthermore, for the sake of consistency, all visualizations of impinging spray combustion were performed using the same ambient conditions (i.e., altitude conditions) and injection settings as those used for the free spray combustion in Part I. This thorough investigation is expected to widen the fundamental understanding of the detailed physical and chemical processes involved in different wall impingement distances under different altitude conditions, which will be beneficial for the breakthrough of efficient and clean combustion technology for diesel engines in plateau regions.

2. EXPERIMENTAL APPARATUS AND PROCEDURES

For the impingement investigation presented in this work, the experimental apparatus and procedures were essentially similar to those described in Part I of this investigation.[41] Thus, only a brief description is presented in this section about the modifications for CVCC and image processing.

2.1. Optical Chamber and Injection System. The visualization campaign of the impinging spray combustion was carried out in the CVCC used in Part I of this investigation by adding a wall impingement system, as depicted in Figure 1. The major structure of CVCC was a symmetric cube with a length of 380 mm. Inside the CVCC, there was a cubic closed combustion chamber with a length of 136 mm, providing enough space to install the wall impingement system for impinging spray combustion studies. The impingement system is introduced in the next section. The CVCC had six main ports for optical access and injector installation, two of which were installed with quartz glass with a maximum optical diameter of 130 mm and a thickness of 50 mm in line with the light beam to form line-of-sight optical access for visualization. A Bosch model CRIN2 fuel injector with a single sac-type nozzle was vertically mounted at the center of one main port. The diesel fuel was pressurized by a Bosch CP3.3 fuel pump, and the injection duration was maintained at 2.0 ms for all of the tests in order to achieve a quasi-steady-state spray and flame. Prior to performing the visualization experiments, a pre-combustion technique was used to generate a high-temperature, high-pressure environment inside the CVCC to reproduce typical in-engine conditions. The specified density was achieved by metering a combustible mixture of acetylene (C_2H_2), oxygen (O_2), and nitrogen (N_2) entering the chamber. This mixture was then ignited with a spark plug and burned, and thus, its temperature and pressure increased rapidly and then fell gradually. Once the pressure decreased to the precalculated value, the diesel injector was triggered, and the high-speed color camera recorded the impinging spray flame images simultaneously. More detailed information about the CVCC and the procedure for reproducing diesel-like

https://doi.org/10.1021/acsomega.3c07357
ACS Omega 2024, 9, 4513−4527

thermodynamic conditions can be found in Part I of this investigation, and also in previous publications.[35,42]

2.2. Wall Impingement System. As mentioned above, the CVCC system was modified by adding a specially designed wall impingement system. A photograph of this system is shown in Figure 2, which consists of a flat wall, a support post,

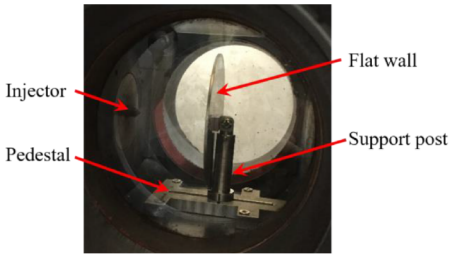

Figure 2. Photograph of the wall impingement system.

and a pedestal. A circular stainless−steel wall design with a diameter of 100 mm was chosen for the flat wall to simulate a piston surface. The flat wall was mounted on a support post so that the wall was opposite the injector and perpendicular to the injector axis, thus generating an impinging spray flame. Moreover, the pedestal attached to the bottom of the chamber was machined with a guide rail that was parallel to the injector axis, and then the support post could move back and forth along the rail to adjust the distance from the injector tip to the flat wall (also referred to as the impingement distance).

2.3. Optical Techniques and Processing Methods. Three standard optical techniques, diffused back-illumination imaging, broadband chemiluminescence imaging, and flame natural luminosity imaging, were still employed to visualize the liquid spray, ignition, and flame progression of the impinging jet, respectively. The camera settings for the three techniques are listed in Table 1. The view area captured by the camera was

Table 1. Details of the Optical Setup for the Employed Techniques

	diffused back-illumination imaging	broadband chemiluminescence imaging	flame natural luminosity imaging
camera	PCO Dimax S1 high-speed color camera		
lens	Tokina 100 mm (f/2.8)		
light source	LED	none	none
filter	None	600 nm low pass	ND8
exposure time (μs)	20	54	4
frame rate (fps)	10 000		
resolution	576 × 648		
scale (mm/pixel)	0.18		

different from that in the free jet case; therefore, the camera settings were adjusted with care to maintain a reasonable spatial resolution. In this work, all images were taken with a resolution of 576 × 648 pixels and a frame rate of 10 000 frames per second.

All the images were processed following a similar procedure to that described in Part I of this investigation. The impinging spray and flame images, after background subtraction, were binarized by a fixed threshold to determine the boundary of the liquid spray and flame zone, and then the macroscopic parameters of interest were extracted to characterize the spray flame progression. In addition to the parameters mentioned in Part I of this investigation such as flame area, spatially integrated natural luminosity (SINL), and time integrated natural luminosity (TINL), some parameters characterizing the spray and flame after impingement were defined in this work, as shown in Figure 3. For the impinging liquid spray, the liquid

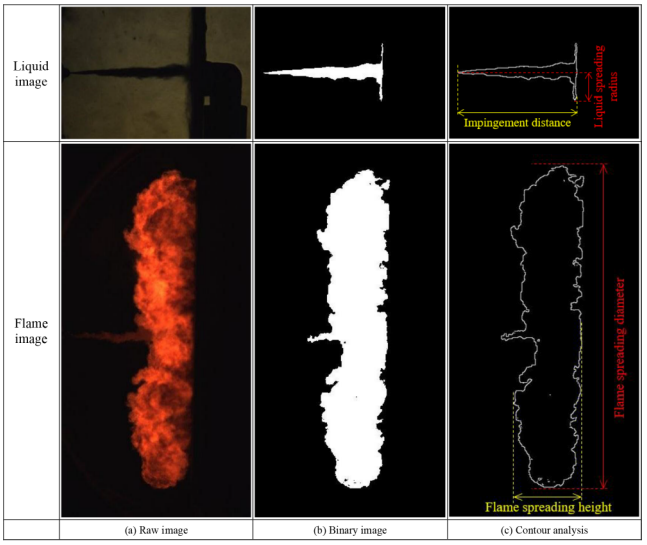

Figure 3. Image processing and parameter definition.

phase penetration after impingement was taken as the sum of the impingement distance and liquid spreading radius along the wall surface. For the impinging flame, the flame spreading height represented the axial expansion of the flame spreading in the direction perpendicular to the wall, and the flame spreading diameter was an indicator reflecting the radial expansion parallel to the wall surface. Sensitivity analysis to the threshold was performed to confirm that the values of the employed parameters did not change with the specific threshold. The ignition images were processed with standard processing methodology, in which the ignition threshold was selected as 50% of the magnitude of the high-temperature chemiluminescence level to determine the appearance and locations of the ignition kernels, and then the ignition delay and ignition distance could be calculated.

2.4. Experimental Conditions. Details of the experimental conditions are listed in Table 2. The ambient densities were selected to closely represent the in-cylinder densities of the prototype engine at the start of fuel injection when

Table 2. Test Conditions

fuel	#0 diesel fuel		
fuel density (kg/m^3)	835		
injector type	single-hole		
nozzle diameter (mm)	0.32		
injection pressure (MPa)	90		
injection duration (ms)	2.0		
impingement distance (mm)	37, 57, 77		
ambient temperature (K)	800		
ambient pressure (MPa)	3.69	3.05	2.61
ambient density (kg/m^3)	16.07	13.31	11.37
simulated altitude (m)	0	3000	4500

https://doi.org/10.1021/acsomega.3c07357
ACS Omega 2024, 9, 4513−4527

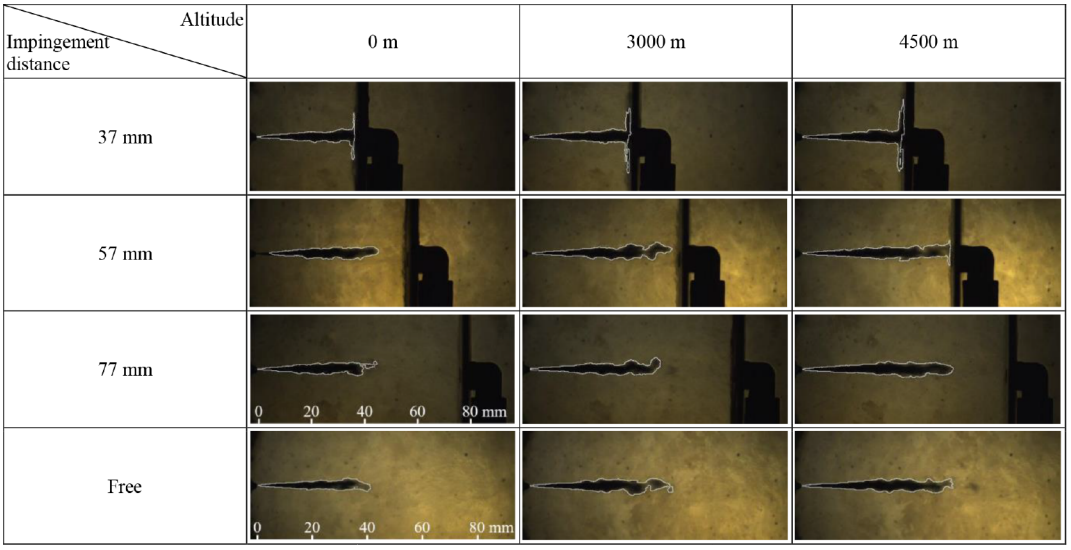

Figure 4. Liquid spray morphology under different altitude conditions (1.5 ms ASOI).

operating under the altitude conditions of 0, 3000, and 4500 m. The nozzle diameter of the injector and the injection pressure were determined by referring to a realistic injection system. The impingement distance was adjusted from 77 to 37 mm to reproduce the transition from a free jet to an impinging jet (refer to JWI) up to liquid impingement (refer to SWI). The choice of 57 mm for impingement distance was corresponding to the distance from the injector tip to the piston bowl wall of the prototype engine at the time of injection. Likewise, visualizations under three altitude conditions were performed at every impingement distance, and the free jet visualizations under identical altitude conditions in Part I of this investigation will be recalled for comparison, aiming to obtain detailed information about the role of the altitude combined with different impingement distances. Meanwhile, each test condition was repeated at least five times to ensure the experimental reliability and repeatability.

3. RESULTS AND DISCUSSION

3.1. Liquid Spray Characteristics. *3.1.1. Liquid Spray Morphology.* Considering that the liquid fuel penetrated to the farthest location during the quasi-steady period, images of the liquid spray at 1.5 ms after the start of injection (ASOI) are shown in Figure 4 to exhibit the spatial relationships between the liquid spray and the flat wall under all test conditions considered. The white lines represent the boundaries of the liquid spray.

First, let us detail the morphology of liquid spray under different altitude conditions at an impingement distance of 57 mm as an example. In general, the liquid spray penetrated through the area between the nozzle and the flat wall, exhibiting a similar behavior to the free jet as discussed in Part I of this investigation,[41] so the temporal sequences of the liquid spray images for the case of 57 mm impingement distance were not given to save the length of this paper. However, it is interesting to observe the different spatial relationships between the liquid spray and the flat wall at 57 mm impingement distance from Figure 4. Under the altitude condition of 0 m, the liquid fuel had almost completely evaporated before reaching the flat wall and no liquid fuel impinged upon the wall. When the altitude was increased to 3000 m, the liquid fuel penetrated downstream to the near-wall region due to the reduced vaporization rate as the ambient density decreased, causing the detached liquid tip, a similar structure which had been confirmed by Feng et al.,[43] to randomly impinge on the flat wall. As the altitude increased to 4500 m, the vaporization rate of the liquid fuel decreased further, and the liquid spray penetrated further downstream, resulting in the liquid spray intermittently impinging upon the wall without the formation of a continuous wall film.

Next, when the impingement distance was varied, the spatial relationships between the liquid spray and the flat wall became more interesting. Apparently, as the impingement distance decreased from 77 to 57 mm, the liquid spray developed fully, as it did for the free jet, and generally, there was no liquid impingement for all altitudes. However, at an impingement distance of 37 mm, the liquid fuel piled up on and spread along the wall surface with significant liquid impingement on the flat wall under all three altitude conditions. Therefore, it can be concluded that when the impingement distance is long enough (in this work the impingement distance is longer than 77 mm), the impingement event belongs to the JWI regardless of the altitude; as the impingement distance decreases to a certain value (57 mm in this work), the impingement type switches from JWI to SWI; as the impingement distance decreases further (shorter than 37 mm in this work), it always belongs to the SWI for all three altitudes. The above wide range of impingement cases confirms the reasonableness of the selection of test conditions in this work and lay a good foundation for the subsequent comprehensive study of the impinging ignition and combustion characteristics under different altitude conditions.

From another perspective, it is well-known that one practical concern addressed by the liquid spray measurement is the assessment of the liquid spray impingement on the piston bowl walls in diesel engines.[44−46] Based on the extent of the excessive liquid penetration shown in Figure 4, it is reasonable to intuitively extrapolate that the liquid impingement on the piston bowl wall is not a serious concern for heavy-duty, large-bore diesel engines operating in plateau regions up to 3000 m. However, as the altitude was increased up to 4500 m, the likelihood of liquid impingement becomes greater, which is constant with the findings of recent research.[18,47] Of course,

https://doi.org/10.1021/acsomega.3c07357
ACS Omega 2024, 9, 4513−4527

for light-duty, small-bore diesel engines, liquid impingement is always a concern due to the short injector-to-wall distance, even when operating in plain regions.

3.1.2. Liquid-phase Penetration. Figure 5 shows the liquid-phase penetration under all of the considered test conditions.

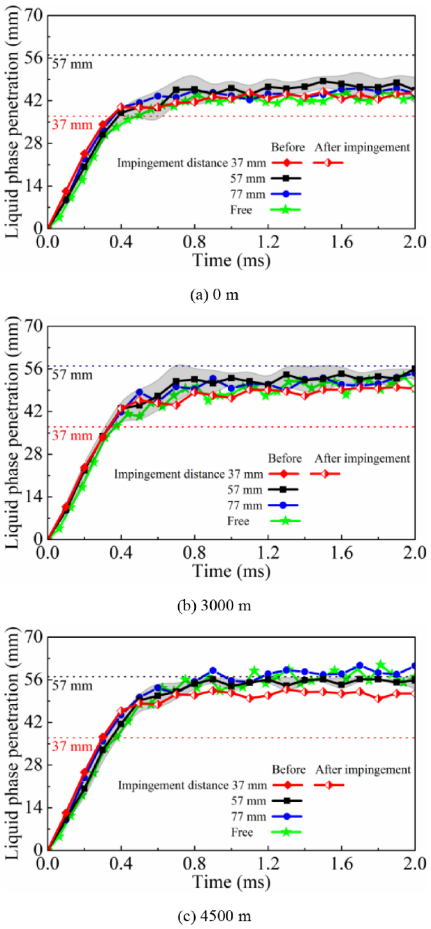

Figure 5. Liquid-phase penetration under different altitude conditions.

For an identical altitude, all liquid-phase penetration curves of the impinging and free jets showed the same growth trend, i.e., after an initial short transient penetration period, the liquid spray tip fluctuated about a mean axial location while the fuel injection continued. It is reasonable to conclude that the overall penetration trend of the liquid spray for an identical altitude was independent of either the presence of the flat wall or the occurrence of the liquid impingement.

Furthermore, since turbulence caused the liquid spray tip to oscillate by a few millimeters about a fixed axial location, the curves of the impinging jets at impingement distances of 77 and 57 mm seemed to intertwine with that of the free jet for all three altitudes. When the impingement distance was decreased to 37 mm, the spacing differences between adjacent penetration curves were negligible under the altitude condition of 0 m, whereas the differences became significant as the altitude was increased to 4500 m. In the next subsection, the liquid length is analyzed to quantitatively reveal the effect of the impingement distance under different altitude conditions.

3.1.3. Liquid Length. Figure 6 shows the liquid lengths for all test conditions considered. Contrary to the monotonic correlation with the altitude for both impinging and free jets,

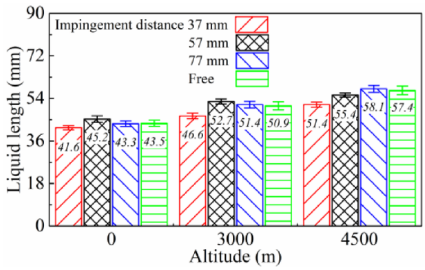

Figure 6. Liquid length under different altitude conditions.

the liquid length was affected by the impingement distance in a rather complicated way under different altitude conditions.

Under the condition of 0 m altitude, the observations were as follows:

a) When the impingement distance was 77 mm, the liquid length was almost the same as that of the free spray.
b) As the impingement distance was decreased to 57 mm, the liquid length increased slightly, which was presumably due to the weaker fuel−air mixing in the central part of the fuel spray upstream of the flat wall,[28] indicating that the liquid penetration may have been affected by the presence of the flat wall even without liquid wall impingement.
c) When the impingement distance was decreased to 37 mm, the liquid length decreased significantly due to the mass and momentum losses by liquid impingement.

The variation of the liquid length for impingement distances under the condition of 3000 m altitude followed the same trend. As the altitude was increased to 4500 m, the major discrepancy in the variation trend was that when the impingement distance was decreased from 77 to 57 mm, the liquid length began to decrease, which was attributed to the mass and momentum losses by intermittent liquid impingement at 57 mm, as described in Section 3.1.1.

In summary, the variation of the liquid length with the impingement distance under identical altitude conditions depended on whether the liquid fuel impinged on the wall. In detail:

a) When the impingement distance was sufficiently long, the liquid length of the impinging jet was comparable to that of the free jet.
b) When the impingement distance was decreased without liquid impingement, the fuel−air mixing process upstream of the flat wall played a certain role in the liquid length.
c) After the liquid impingement, either intermittent or continuous, the liquid length was mainly controlled by the mass and momentum losses.

3.2. Ignition Characteristics. *3.2.1. Ignition Morphology.* The broadband chemiluminescence images at ignition timing for all considered test conditions, which were simultaneously superimposed with the liquid spray image at the same time, are summarized in Figure 7. The red lines represent the boundaries of the ignition kernels, and the white lines represent the boundaries of the liquid spray.

The ignition morphology at an impingement distance of 57 mm was still analyzed first as an example. In this case, the ignition process was characterized by an initial onset of a low-temperature reaction emitting so-called cool-flame chemiluminescence, followed by high-temperature ignition,[48] which was

https://doi.org/10.1021/acsomega.3c07357
ACS Omega 2024, 9, 4513−4527

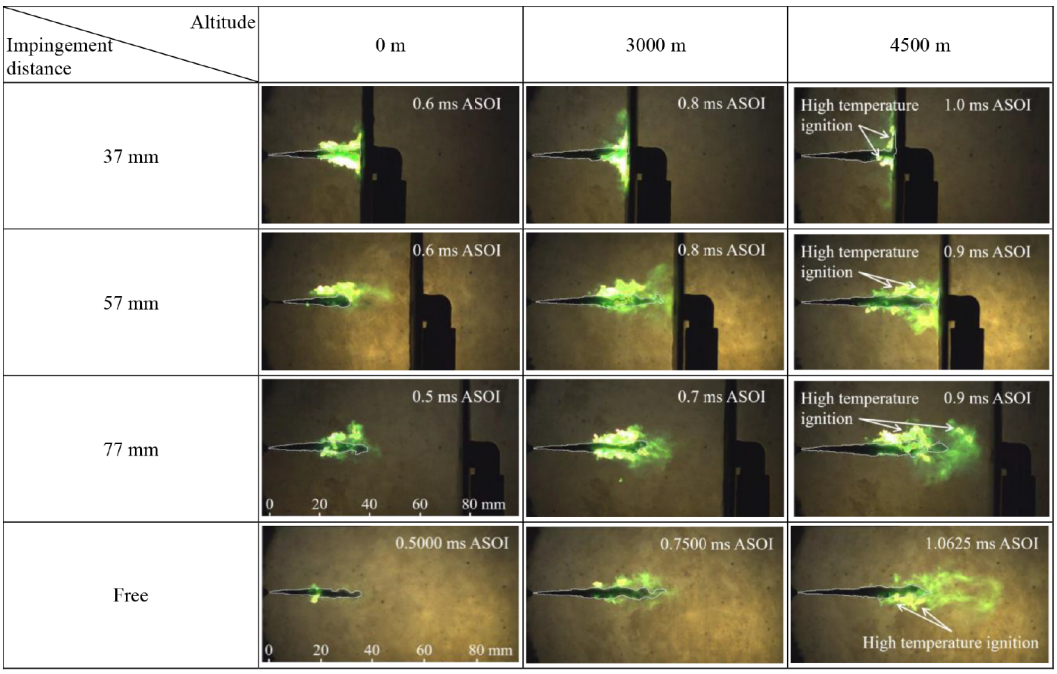

Figure 7. Ignition morphology under different altitude conditions.

similar to the free jet as discussed in Part I of this investigation. However, it should be noted that the ignition region approached the wall more closely with increasing altitude, and some ignition kernels were even located near the wall surface when the altitude was increased to 4500 m. The presence of the flat wall restricted the downstream propagation of the ignitable mixture under higher altitude conditions, which could be regarded as a consequence of the restricted propagation of the liquid spray.

Then the impingement distance was varied. Intuitively, the ignition kernels of impinging jet under an identical altitude condition exhibited an irregular spatial pattern, with variations in location and shape, verifying the inherently stochastic behavior of the impinging ignition,[49] especially higher altitude conditions. When the impingement distance was decreased from 77 to 55 mm, the ignition kernels were mainly distributed at the outer periphery of the liquid spray in the free region of the impinging jet and away from the flat wall, except for the case of an impingement distance of 57 mm and an altitude of 4500 m, where some kernels approached the wall surface around the impingement point. This could be attributed to the intermittent impingement of liquid spray tip upon the flat, as discussed in Section 3.1.1, which promoted the secondary atomization and the re-bound of droplets.[50] When the impingement distance was further decreased to 37 mm, the liquid impingement occurred for all three altitudes, which allowed the ignitable mixture to accumulate in a large range near the wall surface, enhancing the formation of a radical pool in subsequent chemical reactions, and thus, some kernels were even very close to the wall surface.

The above-mentioned near-wall ignition process would have a heavy impact on subsequent combustion and emissions. Next, the ignition delay and ignition distance are introduced as macroscopic parameters for the quantitative analysis of the impinging ignition morphology.

3.2.2. Ignition Delay. The ignition delay under all test conditions considered can be seen in Figure 8. For all the jets,

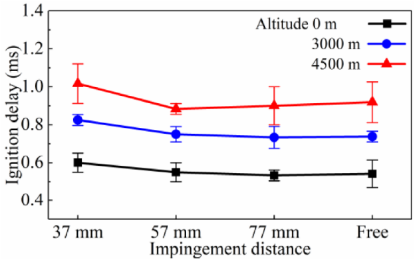

Figure 8. Ignition delay under different altitude conditions.

the ignition delay increased with altitude, mainly due to the poor fuel−air mixing and lower chemical−kinetic reaction rate caused by the smaller ambient density.[44,51] For an identical altitude, when the impingement distance was decreased from 77 to 55 mm, there was no liquid-wall impingement and the ignition delay changed little. When the impingement distance was further decreased to 37 mm, the ignition delay increased significantly, which was speculated to be due to the liquid spray impingement on the flat wall resulting in wall-wetting, which hindered the heat transfer from the flat wall to the fuel−air mixture and consequently reduced the chemical reaction rate. Meanwhile, this increment was amplified with increasing altitude due to more severe liquid impingement. This implied that the liquid impingement affected the ignition timing with significant intensification under higher altitude conditions.

3.2.3. Ignition Distance. Figure 9 presents the ignition distances for all test conditions considered. The effect of the impingement distance on the ignition distance was different under different altitude conditions. For the altitudes of 0 and 3000 m, the ignition distance increased slightly as the impingement distance was decreased, which can be explained by the conjecture that the impingement promoted the mixing of the fuel vapor and air near the flat wall; hence, the ignitable mixture was distributed closer to the wall. However, with the condition of 4500 m altitude, as the impingement distance was decreased, the ignition distance first decreased and then

https://doi.org/10.1021/acsomega.3c07357
ACS Omega 2024, 9, 4513−4527

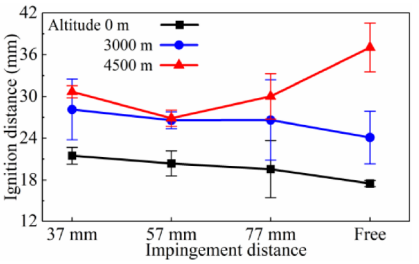

Figure 9. Ignition distance under different altitude conditions.

increased. It can be speculated that for the free jet, the spray fully developed and the ignition occurred at a far downstream location, whereas for the impinging jet, the restriction effect of the flat wall resulted in the decrease in the ignition distance compared with that of the free jet. However, when the impingement distance was decreased from 57 to 37 mm, the severe liquid impingement caused the ignition kernels to be distributed mainly closer to the wall, which can be seen from Figure 7, and therefore the ignition distance seemed to increase instead. Overall, the presence of the flat wall significantly affected the position of the ignition kernels and this effect was more sensitive to the altitude.

3.3. Flame Characteristics. *3.3.1. Flame Morphology.* The flame morphologies at different impingement distances are presented in Figure 10 only for the altitude of 4500 m, as the results were approximately the same for 0 and 3000 m altitudes. Intuitively, the overall flame morphology varied significantly with the change in the impingement distance. Specifically, the results were as follows:

a) For free spray combustion as discussed in Part I of this investigation, the flame could be regarded fully developed, and a lifted flame pattern appeared both before and after the end of the fuel injection, as shown in the images at 1.5 and 2.5 ms ASOI. In the later stage of combustion, such as the image at 3.5 ms ASOI, the flame clung to the end wall of the chamber.

b) For the impinging jet at an impingement distance of 77 mm, driven by the momentum from the fuel injection, the flame propagated downward to impinge on the flat wall and then spread radially along the wall surface with the impingement point as the center. In the upstream region, the flame remained lifted, as it was for the free flame. At the same time, in the downstream region, the flame spread out radially along the wall surface with the impingement point as the center. In the later stage of combustion, the upstream lifted flame region shrank because there was no fuel supply, and the peripheral edge of the downstream flame rose due to the rolling-up motion caused by the wall jet vortex. As a result, the convex shape in the vicinity of the impinging flame's axis became no longer visible.

c) With respect to the impingement distance of 57 mm, the flame also impinged continuously on the flat wall. As the momentum remained large, the flame–wall impingement resulted in a strong vortex in the wall jet region. It is interesting to note that the flame upstream no longer formed a stable lifted flame as it did for a free flame but rather presented a convex shape in the vicinity of its axis overall both before and after the end of the fuel injection. As time passed, the flame changed from convex to concave in the vicinity of its axis due to the

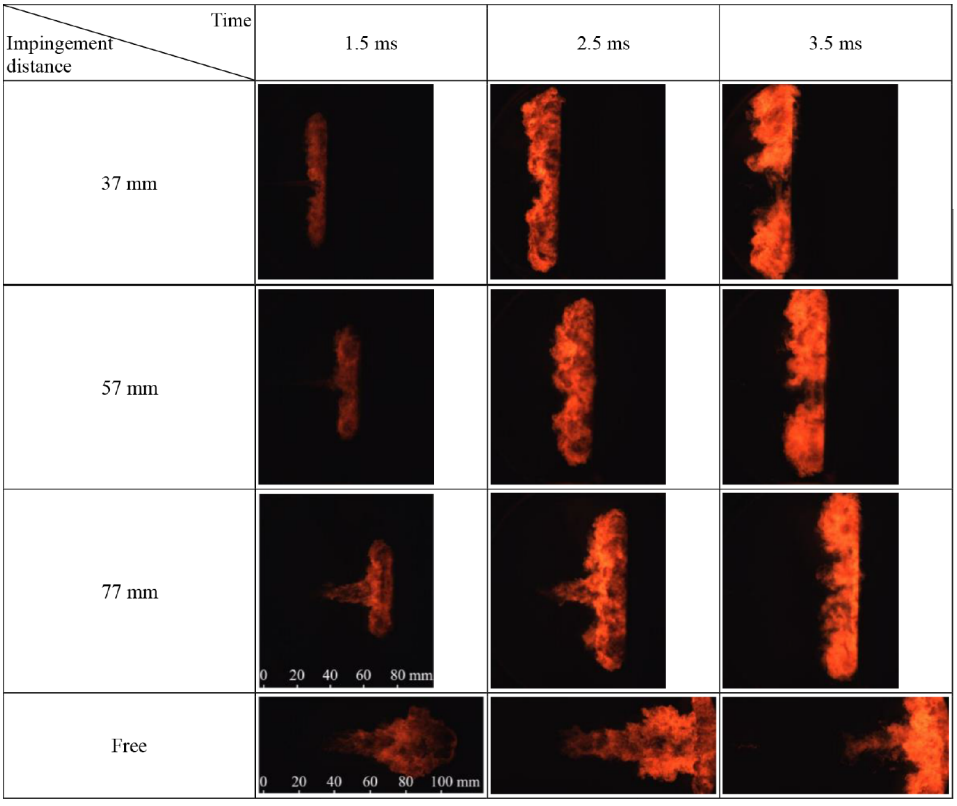

Figure 10. Flame morphology under an altitude condition of 4500 m.

https://doi.org/10.1021/acsomega.3c07357
ACS Omega 2024, 9, 4513−4527

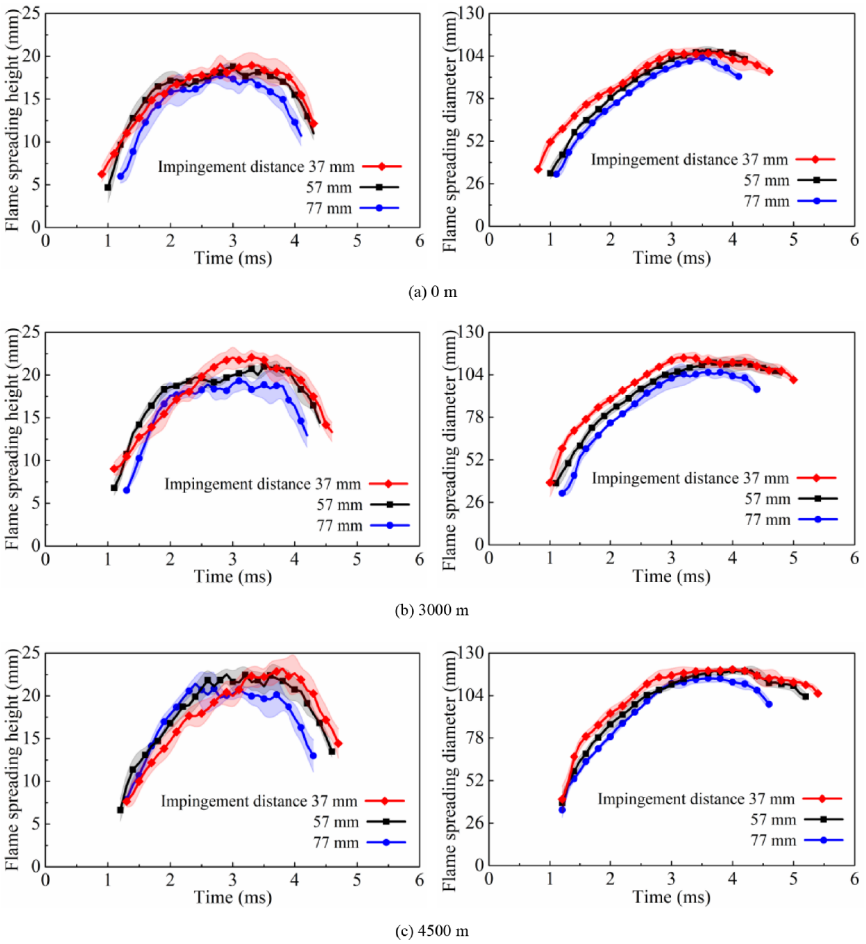

Figure 11. Flame spreading height (left) and diameter (right) under different altitude conditions.

cutoff of the fuel injection. Note again that the flame morphology at an impingement distance of 57 mm for all three altitudes all exhibited essentially the pattern of a disc flame,[52] which was totally different from the lifted pattern of the free flame discussed in Part I of this investigation.

d) For the impingement distance of 37 mm, the flame−wall interactions were already fully established shortly after the initial flame appearance, and the smaller amount of momentum loss prior to impingement allowed more spray and flame to be pushed downward along the flat wall surface, resulting in a strong vortex at the flame tip. Thus, the impinging flame appeared with a concave shape, even before the end of the fuel injection. As time elapsed, the impinging flame exhibited a more prominent concave shape. In the later stage of combustion, the flame in the impingement region disappeared, leaving two isolated flame areas in the wall jet vortex region.

3.3.2. Flame Spreading Height and Diameter. The effects of the impingement distance on the flame spreading height and diameter under different altitude conditions are given in the left- and right-hand columns of Figure 11. For each altitude, the impinging flame at different impingement distances of 77, 57, and 37 mm shared the same growth trend; that is, the height and diameter both increased and then decreased with elapsed time after impingement. Thus, the growth trend of the flame after impingement was consistent regardless of the impingement distance. In addition, as the impingement distance was decreased from 77 to 37 mm, the height and diameter both increased overall. This can be explained as the momentum of the flame after impingement increasing due to the smaller amount of momentum dissipation when the jet traveled through the shorter distance from the nozzle to the flat wall. Therefore, the stronger wall jet vortex allowed wider dispersion of the impinging flame in directions perpendicular and parallel to the wall surface.

3.3.3. Flame Area. Figure 12 shows the effect of the impingement distance on the flame area under different altitude conditions. Two significant tendencies are discussed below.

1) For an identical altitude, the flame area exhibited little difference at different impingement distances. A possible reason was as follows. When the impingement distance was decreased from 77 to 37 mm, the flame spreading height and diameter, as shown in Figure 11, both increased overall, while the flame morphology shifted from a convex shape to a concave shape in the vicinity of its axis. These two opposing effects eventually led to a neutral effect of the impingement distance on the flame area. This implied that the impingement distance had little influence on the flame area regardless of the altitude.

2) The flame area curves of the impinging jets exhibited distinguishable differences from those of the free jet under different altitude conditions. Under the condition

https://doi.org/10.1021/acsomega.3c07357
ACS Omega 2024, 9, 4513−4527

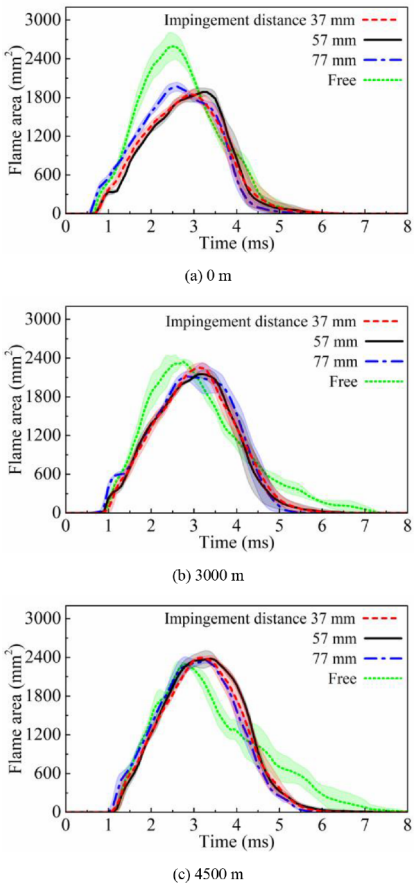

Figure 12. Flame area under different altitude conditions.

of 0 m altitude, the impinging flame, which resembled a disc, was confined to the surface of the flat wall, whereas the lifted pattern of the free flame allowed a large distribution of the flame in the upstream region, so the area of the impinging flame was much smaller than that of the free flame during the early stage of combustion. However, in the later stage of combustion, the similar oxidation rates of the impinging and free jets resulted in a sharp decrease in the flame area, and all of the curves of the impinging and free jets seemed to be indistinguishable. When the altitude was increased to 4500 m, in the early stage of combustion, the longer lift-off length of the free flame narrowed the distribution of the flame in the upstream region, presenting a similar area to those of the impinging jets. At a later stage of combustion, the flame area of the impinging jets shrank quickly due to the enhanced air entrainment by the wall jet region, while the free flame clung to the end wall of the chamber, and the flame area decreased slowly due to the poor air entrainment and cooling effect by the wall heat transfer.[48] Interestingly, the curves of the flame area under the conditions of 3000 m altitude exhibited differences in both the early and later stages of combustion. In general, it can be speculated that the difference in the flame morphology between the impinging and free jets mainly influenced the flame area in the early stage of combustion under lower altitude conditions, while under higher altitude conditions, this influence shifted to a later stage of combustion.

The flame morphology is considered to be directly associated with the spatial distribution of the fuel−air mixture,[29,53] and this kind of association will be discussed in detail in the following sections.

3.4. Soot Characteristics. *3.4.1. SINL.* Figure 13 shows the SINLs for all of the test conditions considered. It is

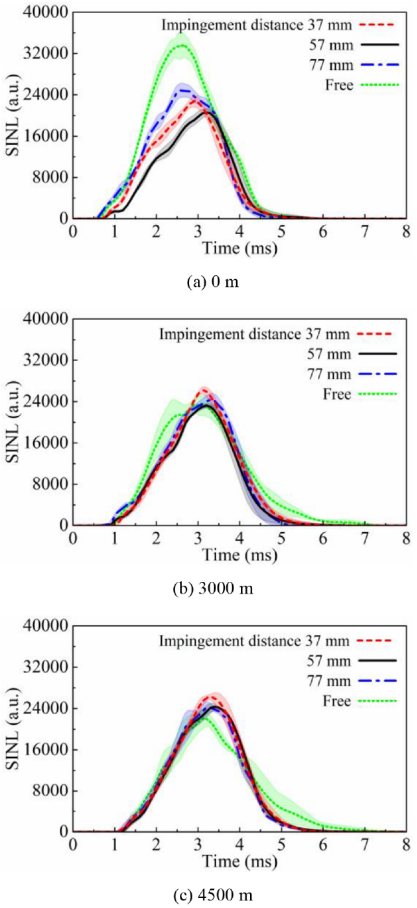

Figure 13. SINL under different altitude conditions.

apparent that the variation in SINL was analogous to that of the flame area in Figure 12. As the flame luminosity came from soot radiation, the larger the flame area was, the more soot formed, and generally the stronger the flame luminosity was. Thus, it can be concluded that the SINLs of the impinging flame at different impingement distances were all directly affected by the flame distribution, as was the SINLs of the free flame as discussed in Part I of this investigation.

However, one major difference in the trend between the SINL and the flame area was that when the impingement distance was decreased from 57 to 37 mm under the same altitude condition, the flame area changed a little, while the peak SINL value increased significantly. The liquid−wall impingement was responsible for this difference. When the impingement distance was decreased to 37 mm, the severe liquid−wall impingement shown in Figure 4 resulted in the formation of a fuel film deposited on the wall surface, and the film formed a pool flame during the spray combustion process, leading to a high level of soot formation.[38]

3.4.2. TINL. Figure 14 brings together the TINLs for all test conditions considered. Under the condition of 0 m altitude, the following observations were made:

https://doi.org/10.1021/acsomega.3c07357
ACS Omega 2024, 9, 4513−4527

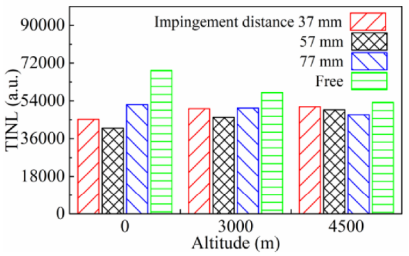

Figure 14. TINL under different altitude conditions.

a) When the impingement distance was 77 mm, the impinging flame in the upstream region remained lifted, as it was for the free flame. However, in the downstream zone, the flame impinged upon the wall, resulting in an intensity vortex larger than that of the free flame in the flame head region. Hence, the impinging flame entrained more ambient gas than the free flame. As a result, the TINL of the impinging flame at the impingement distance of 77 mm was smaller than that of the free flame.

b) As the impingement distance was decreased to 57 mm, the smaller amount of momentum dissipation prior to impingement allowed a larger intensity vortex in the flame head region, leading to a smaller TINL than that of the impinging flame at 77 mm.

c) When the impingement distance was further decreased to 37 mm, the liquid spray impinged upon the wall and deposited to form a wall film, which led to the occurrence of a pool fire and hence increased soot formation, manifesting as a higher TINL.

The same tendency was observed under the condition of 3000 m altitude. However, when the altitude was increased to 4500 m, the only difference was that the TINL of the impinging flame at the impingement distance of 57 mm was larger than that of 77 mm, which was most likely caused by the pool flame of the adhered film on the wall surface that resulted from the intermittent liquid−wall impingement at 57 mm. This explanation can be supported by the decrease in the liquid length when the impingement distance was decreased from 77 to 57 mm, as discussed in Section 3.2.1. Furthermore, according to the above trends observed in Figure 14, it is speculated that in terms of the more complete combustion and lower soot emissions, there was an optimal impingement distance for each altitude, and the higher the altitude, the longer the optimal impingement distance was.

It is also worth remarking that Figure 14 provides some useful insights into the opposite effect of the altitude on the TINL for different impingement distances. As discussed in Part I of this investigation, the decrease in the TINL of the free flame with increasing altitude was mainly due to the longer flame lift-off length, which resulted in more air entrainment upstream of the lifted flame. The TINL of the impinging flame at an impingement distance of 77 mm, which maintained a similar lifted flame pattern in the upstream region, shared the same trend as that of the free flame. However, when the impingement distance was decreased to 57 and 37 mm, the impinging flame formed a disc pattern instead of the lifted pattern, which diminished the ability of air entrainment and fuel−air mixing upstream of the lifted flame, allowing the global ambient entrainment and fuel−air mixing to play a dominant role on the ensuing flame combustion. As a result, the TINL of the impinging flame at both 57 and 37 mm increased with the increase in altitude due to the decreased ambient density. The above analysis clarified the essential difference in the ambient entrainment and mixing between the impinging and free spray combustion,[22,54] further confirming the decisive effect of the flame morphology.

4. ROLE OF ALTITUDE IN SPRAY COMBUSTION PROCESS OF IMPINGING DIESEL JET

As outlined in the Introduction, a key aspect of this work was to move from an unlimited domain to a limited one, where the latter physically and chemically resembles more closely the real in-cylinder conditions of a diesel engine. In the preceding sections, the combined results from the visualizations with the variation of the altitudes and impingement distances, as well as the comparison with the free jet, widened the basic physical and chemical understanding of the impinging spray combustion under different altitude conditions. In this section, based on the philosophy in Part I of this investigation,[41] the rather detailed information on the altitude and impingement distance allowed the schematic diagram proposed by Siebers and Higgins[55] to be extended to the impinging jet, leading to a schematic description of the spray flame structure, as shown in Figure 15 for a jet impinging on a perpendicular flat wall

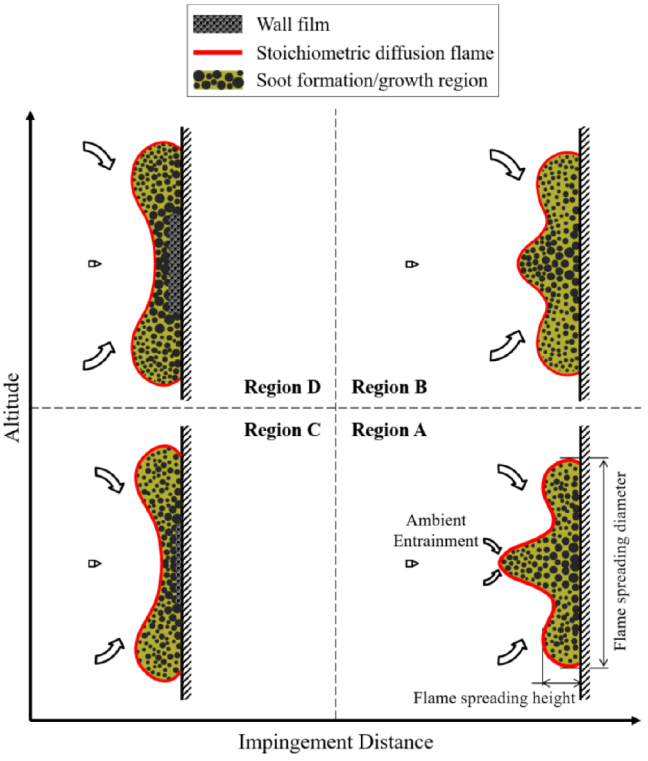

Figure 15. Schematic diagram depicting the spray flame structure of the impinging jet under different altitude conditions.

during the stabilized diffusion phase. The horizontal axis corresponds to the impingement distance, increasing from left to right. The vertical axis corresponds to the altitude, increasing from the bottom to top. To clarify the role of the altitude in the impinging spray combustion process combined with different situations of wall impingement, the spray flame structures in four typical regions are compared, namely, long impingement distance and low altitude condition (Region A),

https://doi.org/10.1021/acsomega.3c07357
ACS Omega 2024, 9, 4513−4527

long impingement distance and high altitude condition (Region B), short impingement distance and low altitude condition (Region C), and short impingement distance and high altitude condition (Region D).

The right column in Figure 15 is discussed first, where the impingement distance is long enough that the extent of the wall interaction is weak and no liquid spray impinges on the wall. When the altitude is low in Region A, the upstream of the flame remains lifted, as it was for the free flame, and in the downstream zone, the flame spreads out radially along the wall surface. The flame−wall impingement results in a strong vortex in the wall jet region, allowing more ambient gas entrainment and, thus, a low soot level for the impinging flame than for the free flame under the same ambient conditions. Upon further increasing the altitude into Region B, the resistance decreases due to the smaller ambient density. As a result, the initial flame appears further downstream and closer to the flat wall, and then, the lifted pattern in the upstream region of the impinging flame becomes less evident. At the same time, the vortex in the wall jet region becomes stronger due to the smaller dissipation of momentum. Therefore, the flame morphology presents a convex shape in the vicinity of its axis overall, and the global ambient entrainment and fuel−air mixing play dominant roles in the ensuing flame combustion.

Next, the left column in Figure 15 is considered where the impingement distance is short, yielding intensified wall interactions and significant liquid−wall impingement. As depicted in Region C, the flame−wall interactions are fully established shortly after the initial flame appearance, so the flame in the upstream region is no longer distinguishable as a lifted pattern. Compared to the case of a long impingement distance in Region A, the short impingement distance reduces the dissipation of momentum before the impingement, which, in turn, leads to a stronger vortex at the flame tip after impingement. Therefore, the impinging flame in Region C exhibits a distinct concave shape in the vicinity of its axis overall, and the global ambient entrainment and fuel−air mixing dominate the ensuing flame combustion. In addition, a wall film forms after liquid impingement and results in a pool fire, which is favorable for soot formation. Finally, after increasing the altitude into Region D, the momentum dissipation further decreases due to the smaller ambient density, enhancing the vortex in the wall jet region. However, the most critical factor resulting in soot emission is that the smaller ambient density also enhances the excessive liquid penetration, and consequently, the pool fire is intensified by more fuel adhesion on the wall, leading to a higher level of soot formation.

The schematic above is highly simplified, and it attempts to depict changes of the liquid−wall interactions and impinging flame morphology under different altitude conditions only based on the results discussed in this work. However, it can furnish the diesel engine community with a mental image to promote new thinking beyond the popular solutions, such as two-stage turbocharger systems,[56−58] alternative fuels,[59−61] oxygen enrichment of the intake air,[62−64] adjusted injection systems,[65−67] and advanced injection strategies,[68−70] to recover and improve the performance of diesel engines operating in plateau regions. Herein, we attempt to analyze two viewpoints.

(a) Optimal impingement distance. As commented in the Introduction, the liquid−wall impingement was verified to significantly worsen the combustion and emissions of high−altitude diesel engines, and thus, the liquid impingement avoidance has become an agreed upon strategy. Currently, one of the traditional and practical methods to reduce the liquid length is to decrease the nozzle diameter, which is limited by the critical peak load capability for heavy-duty diesel engines. Alternatively, adjusting the impingement distance can also avoid liquid impingement, which has been rarely considered, because the distance between the injector tip and chamber wall is always fixed. However, in this investigation, it was found that a longer impingement distance is not necessarily better; that is, there is an optimal impingement distance for soot minimization. This agrees with the conclusion made by Li et al.[38] As a consequence, the tendency of the liquid length and the optimal impingement distance to both increase with increasing altitude provides additional guidance on the design and selection of related components for high-altitude diesel engines.

(b) Better air utilization throughout the combustion chamber. It is well-known that the reduction of the air density inhaled into the cylinder is the essential reason for the performance deterioration of diesel engines operating in plateau regions. In addition to the efforts to increase the intake air amount, it is also helpful to improve air utilization throughout the combustion chamber. As discussed previously, the spreading height and diameter of the flame after impingement both increased under higher altitude conditions. For the heavy-duty diesel engine prototype targeted in this investigation, the piston bowl shape resembled the letter "ω" and the flame impinged upon the edge of the piston bowl.[21] After impingement, the long-penetrated flame spread out to the sides and folded back toward the center of the bowl, during which the wing of the flame inevitably contacted the wings of the adjacent flames, and a stagnation surface was established, facilitating soot formation.[29] In other words, the vortex in the wall jet region, which was shown to be conducive to the ambient entrainment and fuel−air mixing, would be diminished due to plume-to-plume interactions, weakening the benefits of a longer penetrating flame with increasing altitude for air utilization throughout the combustion chamber. The fixed spray orientation of the fixed injection system complicated the corresponding optimization. Alternatively, the piston shape could be redesigned to redirect the flame in the radial direction and then gradually back toward the central region of the piston bowl, avoiding the plume-to-plume interactions. In this way, the strongest wall jet vortex can be formed for better air utilization and thus improved chemical−kinetic reactions, which are also conducive to soot reduction. Recently, some innovative piston designs, such as the lateral swirl combustion system (LSCS) developed by Beijing Institute of Technology,[71] and the wave piston patented by Volvo,[72] have offered promising approaches for diesel engine applications in plateau regions.

It is essential to recognize that the advantages and disadvantages of high jet penetration are largely dependent on the diesel engine size and design, and ultimately, the goal of any combustion system is to achieve as much utilization of in-cylinder air as possible, leading to more complete combustion, especially for high-altitude diesel engines. It is the authors' hope that the fundamental information from this investigation can be applied to the technological changes that inevitably occur during future diesel engine evolution to achieve efficient and clean combustion for diesel engines in plateau regions.

https://doi.org/10.1021/acsomega.3c07357
ACS Omega 2024, 9, 4513−4527

5. SUMMARY AND CONCLUSIONS

In this work, the impinging spray combustion evolution of heavy-duty diesel engines operating under different altitude conditions was thoroughly investigated in a CVCC. The impingement distance was adjusted to cover different situations of wall impingement. The following conclusions can be drawn.

1) For an identical altitude, the growth pattern of the liquid spray was independent of either the presence of the flat wall or the occurrence of the liquid impingement. However, the latter, whether intermittent or continuous, was responsible for the reduction of the liquid length due to mass and momentum losses.
2) With the decrease in impingement distance, the ignition delay changed little until the liquid spray impinged on the wall and then the ignition delay increased, especially under higher altitude conditions. The effect of the impingement distance on the ignition distance was more sensitive to the altitude; under the altitude conditions of 0 and 3500 m, the ignition distance exhibited a slight increase; while under the condition of 4500 m altitude it first decreased and then increased.
3) The impinging flame exhibited the pattern of a disc flame. Although it made larger size of the spreading flame by the more vigorous wall jet vortex, the decreased impingement distance had a neutral effect on the flame area, presumably due to the shrinkage in the flame upstream area as the flame morphology shifted from a convex to a concave shape. The curves of the SINL duplicated the tendency of the flame area curves, with one major discrepancy being that the peak SINL at the impingement distance of 37 mm increased significantly for all altitudes, which was attributed to the pool fire resulting from the liquid impingement.
4) When the TINLs for all test conditions considered were pooled together, the TINL apparently first decreased and then increased as the impingement distance was decreased under an identical altitude condition, implying that there was an optimal impingement distance to achieve minimum soot emissions for diesel engines operating at any altitude. The higher the altitude, the longer the optimal impingement distance became.
5) The TINL of impinging flame at 77 mm impingement distance decreased with increasing altitude, which shared the same trend as that of the free flame, mainly due to the longer flame lift-off length. However, when the impingement distance was decreased to 57 and 37 mm, the disc pattern of impinging flame diminished the ability of air entrainment and fuel−air mixing upstream of the lifted flame, therefore the TINL increased with the increase in altitude. The inconsistent tendency in TINL with altitude for the impinging flame at different impingement distances further confirmed the decisive effect of the flame morphology on the ambient entrainment and fuel−air mixing under different altitude conditions.
6) Finally, the spray combustion processes of an impinging diesel jet were determined to occur in four typical regions. A schematic diagram depicting the spray flame structure for an impinging diesel jet was proposed to clarify the role of the altitude in the impinging spray combustion process with different impingement distances. Based on this, new perspectives were offered beyond the popular solutions for practices to recover and improve the performances of diesel engines operating in plateau regions.

This series of unique investigations of free and impinging jets facilitates the scientific understanding of diesel spray combustion under different altitude conditions. Future work should enrich this database, providing more visualization information on this topic. An extensive database could fulfill the need for better model validation data, which would help us to understand the fundamental driving mechanisms behind visualization observations. The authors hope that the collaboration between optical diagnostics and simulation models can establish guidelines for the improvement of current engines and the design of future engines operating in plateau regions.

AUTHOR INFORMATION

Corresponding Authors

Tao Wang − *Institute of Intelligent Manufacturing Technology, Shenzhen Polytechnic University, Shenzhen 518055, China;* orcid.org/0000-0002-6946-5899; Email: charlietree@szpu.edu.cn

Diming Lou − *School of Automotive Studies, Tongji University, Shanghai 201804, China*; Email: loudiming@tongji.edu.cn

Authors

Chengguan Wang − *Institute of Intelligent Manufacturing Technology, Shenzhen Polytechnic University, Shenzhen 518055, China; Shenzhen Institutes of Advanced Technology, Chinese Academy of Sciences, Shenzhen 518055, China;* orcid.org/0000-0002-5787-7001

Piqiang Tan − *School of Automotive Studies, Tongji University, Shanghai 201804, China*

Zhiyuan Hu − *School of Automotive Studies, Tongji University, Shanghai 201804, China*

Liang Fang − *School of Automotive Studies, Tongji University, Shanghai 201804, China*

Rong Yang − *College of Mechanical Engineering, Guangxi University, Nanning 530004, China*

Xiaozhi Qi − *Shenzhen Institutes of Advanced Technology, Chinese Academy of Sciences, Shenzhen 518055, China*

Complete contact information is available at: https://pubs.acs.org/10.1021/acsomega.3c07357

Notes

The authors declare no competing financial interest.

ACKNOWLEDGMENTS

The authors would like to appreciate the support of Guangxi Science and Technology Base and Talent Project (no. 2018AD19349).

ABBREVIATIONS

CI	compression ignition
LES	large eddy simulation
CFD	computational fluid dynamics
CVCC	constant volume combustion chamber
SWI	spray wall impingement
JWI	jet wall impingement
SINL	spatially integrated natural luminosity

https://doi.org/10.1021/acsomega.3c07357
ACS Omega 2024, 9, 4513−4527

TINL time integrated natural luminosity
ASOI after start of injection
LSCS lateral swirl combustion system

REFERENCES

(1) Reitz, R. D. Directions in internal combustion engine research. *Combust. Flame* **2013**, *160* (1), 1−8.
(2) Reitz, R. D.; Ogawa, H.; Payri, R.; Fansler, T.; Kokjohn, S.; Moriyoshi, Y.; Agarwal, A. K.; Arcoumanis, D.; Assanis, D.; Bae, C.; Boulouchos, K.; Canakci, M.; Curran, S.; Denbratt, I.; Gavaises, M.; Guenthner, M.; Hasse, C.; Huang, Z.; Ishiyama, T.; Johansson, B.; Johnson, T. V.; Kalghatgi, G.; Koike, M.; Kong, S. C.; Leipertz, A.; Miles, P.; Novella, R.; Onorati, A.; Richter, M.; Shuai, S.; Siebers, D.; Su, W.; Trujillo, M.; Uchida, N.; Vaglieco, B. M.; Wagner, R. M.; Zhao, H. IJER editorial: The future of the internal combustion engine. *Int. J. Engine Res.* **2020**, *21* (1), 3−10.
(3) Xuan, T.; Wang, Y.; Liu, L.; Yang, C.; He, Z.; Wang, Q.; Yao, M. Experimental study on flame structure and soot formation of jet/wall impinging combustion under diesel−like conditions. *Therm. Sci. Eng. Prog.* **2023**, *43*, 102016.
(4) Bermúdez, V.; Serrano, J. R.; Piqueras, P.; Gómez, J.; Bender, S. Analysis of the role of altitude on diesel engine performance and emissions using an atmosphere simulator. *Int. J. Engine Res.* **2017**, *18* (1−2), 105−117.
(5) Peng, Q.; Liu, R.; Zhou, G.; Zhao, X.; Dong, S.; Zhang, Z.; Zhang, H. Summary of Turbocharging as a Waste Heat Recovery System for a Variable Altitude Internal Combustion Engine. *ACS Omega* **2023**, *8* (31), 27932−27952.
(6) Jiao, Y.; Liu, R.; Zhang, Z.; Yang, C.; Zhou, G.; Dong, S.; Liu, W. Comparison of combustion and emission characteristics of a diesel engine fueled with diesel and methanol−Fischer−Tropsch diesel−biodiesel−diesel blends at various altitudes. *Fuel* **2019**, *243*, 52−59.
(7) Liu, Z.; Liu, J. Effect of altitude conditions on combustion and performance of a turbocharged direct−injection diesel engine. *Proc. Inst. Mech. Eng., Part D* **2022**, *236* (4), 582−593.
(8) Szedlmayer, M.; Kweon, C.-B. M. Effect of altitude conditions on combustion and performance of a multi−cylinder turbocharged direct−injection diesel engine. *SAE Tech. Pap.* **2016**.
(9) Agudelo, J.; Agudelo, A.; Pérez, J. Energy and exergy analysis of a light duty diesel engine operating at different altitudes. *Rev. Fac. Ing., Univ. Antioquia* **2009**, No. 48, 45−54.
(10) Wang, X.; Pan, J.; Li, W.; Wei, H.; Pan, M.; Wang, X.; Wu, H. Optical experiments on diesel knock for high altitude engines under spray impingement conditions. *Fuel* **2020**, *278*, 118268.
(11) Wang, X.; Wei, H.; Pan, J.; Hu, Z.; Zheng, Z.; Pan, M. Analysis of diesel knock for high−altitude heavy−duty engines using optical rapid compression machines. *Energies* **2020**, *13* (12), 3080.
(12) Li, H.; Zhang, X.; Li, C.; Cao, R.; Zhu, W.; Li, Y.; Liu, F.; Li, Y. Numerical Study of Knocking Combustion in a Heavy−Duty Engine under Plateau Conditions. *Energies* **2022**, *15* (9), 3083.
(13) Liu, J.; Ge, Y.; Wang, X.; Hao, L.; Tan, J.; Peng, Z.; Zhang, C.; Gong, H.; Huang, Y. On−board measurement of particle numbers and their size distribution from a light−duty diesel vehicle: Influences of VSP and altitude. *J. Environ. Sci.* **2017**, *57*, 238−248.
(14) Giraldo, M.; Huertas, J. I. Real emissions, driving patterns and fuel consumption of in−use diesel buses operating at high altitude. *Transp. Res. Part D: Transp. Environ.* **2019**, *77*, 21−36.
(15) Serrano, J. R.; Piqueras, P.; Abbad, A.; Tabet, R.; Bender, S.; Gómez, J. Impact on reduction of pollutant emissions from passenger cars when replacing Euro 4 with Euro 6d diesel engines considering the altitude influence. *Energies* **2019**, *12* (7), 1278.
(16) Bi, Y.; Yan, J.; Liu, S.; Xiao, B.; Shen, L.; Wang, P.; Nie, X. Study on Diesel Engine Selective Catalytic Reduction Performance at Different Atmospheric Pressures Using the Response Surface Method. *ACS Omega* **2023**, *8* (16), 14549−14557.
(17) Zhang, C.; Li, Y.; Liu, Z.; Liu, J. An investigation of the effect of plateau environment on the soot generation and oxidation in diesel engines. *Energy* **2022**, *253*, 124086.
(18) Meng, Z.; Liu, Z.; Liu, J. Investigation of in−cylinder combustion deterioration of diesel engines in plateau regions. *Fuel* **2022**, *324*, 124824.
(19) Mohaddes, D.; Ihme, M. Wall heat transfer and flame structure transitions in stagnating spray flames. *Proc. Combust. Inst.* **2023**, *39* (2), 2683−2692.
(20) Peraza, J. E.; Payri, R.; Gimeno, J.; Carvallo, C. Analysis of spray/wall impingement using an ECN single−hole injector and a controlled−temperature wall under realistic engine conditions. *Appl. Therm. Eng.* **2022**, *208*, 118167.
(21) Pickett, L. M.; López, J. J. Jet−wall interaction effects on diesel combustion and soot formation. *SAE Tech. Pap.* **2005**.
(22) Zhu, J.; Nishida, K.; Uemura, T. Experimental study on flow fields of fuel droplets and ambient gas of diesel spray−free spray and flat−wall impinging spray. *Atomization Sprays* **2014**, *24* (7), 599−623.
(23) Fattah, I. M. R.; Yip, H. L.; Jiang, Z.; Yuen, A. C. Y.; Yang, W.; Medwell, P. R.; Kook, S.; Yeoh, G. H.; Chan, Q. N. Effects of flame−plane wall impingement on diesel combustion and soot processes. *Fuel* **2019**, *255*, 115726.
(24) Edwards, C. F.; Siebers, D. L.; Hoskin, D. H.. *A study of the autoignition process of a diesel spray via high speed visualization*; SAE transactions, 1992; pp 187−204. .
(25) Liu, L.; Peng, Y.; Huang, L.; Han, C.; Ma, X. Evaluation of impingement effects on high−power diesel engine mixing process with an optimized stochastic combustion model. *Fuel* **2022**, *328*, 125239.
(26) Feng, L.; Wang, Q.; Liu, H.; Cui, Y.; Yang, Z.; Wang, Y.; Yi, W.; Yao, M. Effect of the stagnation plate on PAHs, soot and OH distributions in partially premixed laminar flames fueled with a blend of n−heptane and toluene. *Combust. Flame* **2021**, *227*, 52−64.
(27) Wu, H.; Zhang, L.; Shi, Z.; Li, H.; Xiao, P.; Li, X. Experimental and numerical studies on fuel−film combustion and wall thermal effect of diesel spray. *Appl. Therm. Eng.* **2023**, *219*, 119545.
(28) Bruneaux, G.. *Mixing process in high pressure diesel jets by normalized laser induced exciplex fluorescence part II: Wall impinging versus free jet*; SAE transactions, 2005; pp 1404−1416. .
(29) Gao, J.; Moon, S.; Zhang, Y.; Nishida, K.; Matsumoto, Y. Flame structure of wall−impinging diesel fuel sprays injected by group−hole nozzles. *Combust. Flame* **2009**, *156* (6), 1263−1277.
(30) Yip, H. L.; Fattah, I. M. R.; Yuen, A. C. Y.; Yang, W.; Medwell, P. R.; Kook, S.; Yeoh, G. H; Chan, Q. N. Flame−wall interaction effects on diesel post−injection combustion and soot formation processes. *Energy Fuels* **2019**, *33* (8), 7759−7769.
(31) Dec, J. E.; Tree, D. R.. *Diffusion−flame/wall interactions in a heavy−duty DI diesel engine*; SAE transactions, 2001; pp 1599−1617.
(32) Mancaruso, E.; Sequino, L.; Vaglieco, B. M. Analysis of spray injection in a light duty CR diesel engine supported by non−conventional measurements. *Fuel* **2015**, *158*, 512−522.
(33) Tang, Q.; Liu, H.; Li, M.; Yao, M. Optical study of spray−wall impingement impact on early−injection gasoline partially premixed combustion at low engine load. *Appl. Energy* **2017**, *185*, 708−719.
(34) Goyal, H.; Panthi, N.; AlRamadan, A. S.; Cenker, E.; Magnotti, G. Analysis of energy flows and emission characteristics of conventional diesel and isobaric combustion in an optical engine with laser diagnostics. *Energy* **2023**, *269*, 126859.
(35) Maes, N.; Dam, N.; Somers, B.; Lucchini, T.; D'Errico, G.; Hardy, G.. *Heavy−duty diesel engine spray combustion processes: experiments and numerical simulations*; technical paper, 2018; pp 1−22. .
(36) Chen, B.; Feng, L.; Wang, Y.; Ma, T.; Liu, H.; Geng, C.; Yao, M. Spray and flame characteristics of wall−impinging diesel fuel spray at different wall temperatures and ambient pressures in a constant volume combustion vessel. *Fuel* **2019**, *235*, 416−425.
(37) Wang, X.; Huang, Z.; Zhang, W.; Kuti, O. A.; Nishida, K. Effects of ultra−high injection pressure and micro−hole nozzle on flame structure and soot formation of impinging diesel spray. *Appl. Energy* **2011**, *88* (5), 1620−1628.

https://doi.org/10.1021/acsomega.3c07357
ACS Omega 2024, 9, 4513−4527

(38) Li, K.; Nishida, K.; Ogata, Y.; Shi, B. Effect of flat−wall impingement on diesel spray combustion. *Proc. Inst. Mech. Eng., Part D* **2015**, *229* (5), 535−549.
(39) Zhao, W.; Yan, J.; Gao, S.; Lee, T. H.; Li, X. Spray, Ignition, and Combustion Characteristics of Diesel, Propanol, and Pentanol Blends in a Constant Volume Chamber. *Energy Fuels* **2021**, *35* (20), 16653−16664.
(40) Liu, S.; Chen, R.; Wang, Y.; Chen, Y.; Guo, X.; Huang, H. Spray and Combustion Characteristics of CTL−Diesel Fuel Blends in a Constant−Volume Combustion Chamber. *ACS Omega* **2023**, *8* (19), 16966−16974.
(41) Wang, C.; Qi, X.; Wang, T.; Lou, D.; Tan, P.; Hu, Z.; Fang, L.; Yang, R. Role of Altitude in Influencing the Spray Combustion Characteristics of a Heavy−Duty Diesel Engine in a Constant Volume Combustion Chamber. Part I: Free Diesel Jet. *Energies* **2023**, *16* (12), 4832.
(42) Yan, J.; Gao, S.; Zhao, W.; Lee, T. H. Spray and combustion characteristics of butanol−diesel and hexanol−diesel blends under high−altitude conditions. *Fuel* **2022**, *307*, 121753.
(43) Feng, L.; Sun, X.; Pan, X.; Yi, W.; Cui, Y.; Wang, Y.; Wen, M.; Ming, Z.; Liu, H.; Yao, M. Gasoline spray characteristics using a high pressure common rail diesel injection system by the method of laser induced exciplex fluorescence. *Fuel* **2021**, *302*, 121174.
(44) Espey, C.; Dec, J. E.. *The effect of TDC temperature and density on the liquid−phase fuel penetration in a DI diesel engine*; SAE transactions, 1995; pp 1400−1416. .
(45) Siebers, D. L.. *Scaling liquid−phase fuel penetration in diesel sprays based on mixing−limited vaporization*; SAE transactions, 1999; pp 703−728. .
(46) Eagle, W. E.; Malbec, L.-M.; Musculus, M. P. B. Measurements of liquid length, vapor penetration, ignition delay, and flame lift−off length for the engine combustion network 'spray B'in a 2.34 L heavy−duty optical diesel engine. *SAE Int. J. Engines* **2016**, *9* (2), 910−931.
(47) Liu, J.; Wang, B.; Meng, Z.; Liu, Z. An examination of performance deterioration indicators of diesel engines on the plateau. *Energy* **2023**, *262*, 125587.
(48) Ma, Y.; Huang, S.; Huang, R.; Zhang, Y.; Xu, S. Ignition and combustion characteristics of n−pentanol−diesel blends in a constant volume chamber. *Appl. Energy* **2017**, *185*, 519−530.
(49) Lillo, P. M.; Pickett, L. M.; Persson, H.; Andersson, O.; Kook, S. Diesel spray ignition detection and spatial/temporal correction. *SAE Int. J. Engines* **2012**, *5* (3), 1330−1346.
(50) Akop, M. Z.; Zama, Y.; Furuhata, T.; Arai, M. Experimental investigations on adhered fuel and impinging diesel spray normal to a wall. *Atomization Sprays* **2013**, *23* (3), 211−231.
(51) Wang, C.; Lou, D.; Tan, P.; Hu, Z.; Liu, S.; Yang, Z. Experimental Study on Diesel Spray Characteristics at Different Altitudes. *SAE Tech. Pap.* **2018**.
(52) Zhang, Y.; Bray, K. N. C. Characterization of impinging jet flames. *Combust. Flame* **1999**, *116* (4), 671−674.
(53) Zhang, Z.; Liu, F.; An, Y.; Gao, H.; Du, W.; Gao, Y.; Lou, J. Effect of wall surface temperature on ignition and combustion characteristics of diesel fuel spray impingement. *Appl. Therm. Eng.* **2018**, *137*, 47−53.
(54) Sepret, V.; Bazile, R.; Marchal, M.; Couteau, G. Effect of ambient density and orifice diameter on gas entrainment by a single−hole diesel spray. *Exp. Fluids* **2010**, *49*, 1293−1305.
(55) Siebers, D. L.; Higgins, B.. *Flame lift−off on direct−injection diesel sprays under quiescent conditions*; SAE transactions, 2001; pp 400−421. .
(56) Yang, M.; Gu, Y.; Deng, K.; Yang, Z.; Liu, S. Influence of altitude on two−stage turbocharging system in a heavy−duty diesel engine based on analysis of available flow energy. *Appl. Therm. Eng.* **2018**, *129*, 12−21.
(57) Zhang, H.; Tang, X.; Mu, L.; Shi, L.; Deng, K. Theoretical and experimental investigation of the pressure ratio distribution and the regulation strategy of a two−stage turbocharging system for various altitudes operation. *J. Mech. Sci. Technol.* **2021**, *35*, 1251−1265.
(58) Zhang, Z.; Liu, R.; Zhou, G.; Dong, S.; Liu, Z.; Xia, X.; Liu, G.; Ding, H. Research on nonlinear model predictive control of regulated two−stage turbocharging system of diesel engine at high altitudes. *Energy Sources, Part A* **2022**, *44* (4), 8718−8735.
(59) Ramos, Á; García−Contreras, R.; Armas, O. Performance, combustion timing and emissions from a light duty vehicle at different altitudes fueled with animal fat biodiesel, GTL and diesel fuels. *Appl. Energy* **2016**, *182*, 507−517.
(60) Yan, J.; Gao, S.; Zhao, W.; Lee, T. H. Study of combustion and emission characteristics of a diesel engine fueled with diesel, butanol−diesel and hexanol−diesel mixtures under low intake pressure conditions. *Energy Convers. Manage.* **2021**, *243*, 114273.
(61) Zhao, W.; Yan, J.; Gao, S.; Lee, T. H.; Li, X. The combustion and emission characteristics of a common−rail diesel engine fueled with diesel, propanol, and pentanol blends under low intake pressures. *Fuel* **2022**, *307*, 121692.
(62) Perez, P. L.; Boehman, A. L. Performance of a single−cylinder diesel engine using oxygen−enriched intake air at simulated high−altitude conditions. *Aerosp. Sci. Technol.* **2010**, *14* (2), 83−94.
(63) Rajkumar, K.; Govindarajan, P. Impact of oxygen enriched combustion on the performance of a single cylinder diesel engine. *Front. Energy* **2011**, *5*, 398−403.
(64) Zhang, Z.; Duan, Y.; Douji, L.; Cidan, D.; Hui, J.; Ye, M. Dynamic Optimal Control Strategy of Membrane Oxygen Enrichment for Engine Performance in the Plateau Environment. In *27th International Conference on Automation and Computing (ICAC). IEEE*; IEEE, 2022; pp 1−7. DOI: .
(65) Wang, X.; Guo, M.; He, M.; Gu, C.; Cheng, J. Study on improvement of high power diesel engine performance in plateau environment. *Chin. Intern. Combust. Engine Eng.* **2014**, *35* (2), 113−118.
(66) Ren, Z.; Su, T.; Wang, Z.; Yu, J.; Ding, J. Study of adjusting diesel fuel supply system in plateau area. *Acta Armamentarii* **2015**, *36* (12), 2217−2223.
(67) Tan, P.; Wang, D.; Wang, C.; Li, Y.; Lou, D.; Li, Y.; Liu, S.; Yang, Z. Performance optimization of heavy−duty diesel engine in plateau environment. *Acta Armamentarii* **2018**, *39* (3), 436−443.
(68) Zhu, Z.; Zhang, F.; Li, C.; Wu, T.; Han, K.; Lv, J.; Li, Y.; Xiao, X. Genetic algorithm optimization applied to the fuel supply parameters of diesel engines working at plateau. *Appl. Energy* **2015**, *157*, 789−797.
(69) Wang, J.; Shen, L.; Bi, Y.; Liu, S.; Wan, M. Power recovery of a variable nozzle turbocharged diesel engine at high altitude by response surface methodology and sequential quadratic programming. *Proc. Inst. Mech. Eng., Part D* **2019**, *233* (4), 810−823.
(70) Wang, J.; Shen, L.; Bi, Y.; Lei, J. Modeling and optimization of a light−duty diesel engine at high altitude with a support vector machine and a genetic algorithm. *Fuel* **2021**, *285*, 119137.
(71) Li, X.; Chen, Y.; Su, L.; Liu, F. Effects of lateral swirl combustion chamber geometries on the combustion and emission characteristics of DI diesel engines and a matching method for the combustion chamber geometry. *Fuel* **2018**, *224*, 644−660.
(72) Eismark, J.; Christensen, M.; Andersson, M.; Karlsson, A.; Denbratt, I. Role of fuel properties and piston shape in influencing soot oxidation in heavy−duty low swirl diesel engine combustion. *Fuel* **2019**, *254*, 115568.

https://doi.org/10.1021/acsomega.3c07357
ACS Omega 2024, 9, 4513−4527